Journal of Optoelectronic and Biomedical Materials Vol. 17, No. 4, October-December 2025, p. 291 - 302

Synthesis and characterization of (Fe_2O_3:Al) nanostructures thin films

F. G. Hammoodi *, F. Y. Mohammed, N. I. Ibrahim, Z. T. Khodair
Department of Physics, College of Science-University of Diyala, Diyala, Iraq

In this study, aluminum (Al) doped Fe_2O_3 thin film nanoparticles with varying concentrations were prepared using hydrothermal and spray coating methods. Advanced characterization techniques, including ultraviolet-visible (UV-Vis) spectroscopy, X-ray diffraction (XRD), field emission scanning electron microscopy (FE-SEM), and energy dispersive spectroscopy (EDS), were used to evaluate the optical and morphological properties of the films. Structural studies using X-ray diffraction confirmed the film phase and revealed a polycrystalline structure composed of nanocrystals. FE-SEM was used to verify the morphology. Results showed a typical particle size range of 54 to 36 nanometers. EDS data indicated an Al atomic doping fraction of 6.4% in the Fe_2O_3. Spectrophotometry was used to determine the optical properties of the films, including band gap, transmittance, and absorptivity. Optical analysis revealed an optical band gap of approximately 1.9–2.3 eV in the 340–900 nm wavelength range, which varied with concentration and preparation process. The samples prepared by the spray coating method exhibited a more regular structure, consistent with the structural and optical properties of samples prepared by both methods. Furthermore, it is important to point out that these materials must be considered in a broader context, as they have potential applications in various technological fields.

(Received September 21, 2025; Accepted December 22, 2025)

Keywords: Al-doped Fe_2O_3, nanoparticles, Hydrothermal, Spray pyrolysis method

1. Introduction

The development of technological and scientific applications is greatly aided by the cutting-edge area of nanomaterials research. Materials of nanoscale dimensions between 1 and 100 nanometers are referred to as nanomaterials. This range of dimensions has special characteristics that set it apart from traditional materials. A number of techniques may be used to efficiently prepare these materials; the primary emphasis of this study is on spray and hydrothermal techniques. These techniques enable manipulation of the composition, size, and form of nanomaterials, hence establishing the advantages and disadvantages of each of the previously stated techniques [1-2]. These days, semiconductor metal oxide nanoparticles are appealing because they vary from their bulk counterparts in terms of electric, dielectric, optical, biomedical, photo-catalytic, and magnetic characteristics [3]. Because it is non-toxic, inexpensive, abundant, thermally and chemically stable at room temperature, and environmentally benign, Fe_2O_3 is highly valued [4]. With a rhombohedral crystal structure, a high refractive index, and a direct band gap between 1.9 and 2.2 eV, it is an inherently n-type semiconductor [5]. Numerous electronic and optoelectronic applications, such as gas sensors, vapour sensors, microwaves, high-density recording media, solid-state lithium-ion batteries, supercapacitors, water splitting for hydrogen production, solar cells, and antibacterial coatings, can benefit from the intriguing properties of Fe_2O_3 [6-7]. Aluminum (Al) is a metallic fuel that has traditionally been used as the primary fuel due to its

* Corresponding author: faissal_hammody@uodiyala.edu.iq
https://doi.org/10.15251/JOBM.2025.174.291

high density, good catalytic performance, and low cost; while Fe_2O_3 is a metal oxide that can improve reactivity, and both materials exist in the Fe_2O_3/Al system[8]. Nanostructured composites can also improve reactivity control by changing factors such as shape and particle size[9].

This study examined how the size, shape, and optical band gap of Al:Fe_2O_3 nanoparticles were affected by changes in the concentration of the material employed in their manufacture. The two straightforward methods of spraying and hydrothermal synthesis were used to create (Al:Fe_2O_3) nanoparticles. Using a variety of characterisation techniques, including X-ray diffraction (XRD), field emission scanning electron microscopy (FE-SEM), energy dispersive spectroscopy (EDS), and ultraviolet-visible (UV-Vis) analysis, the nanoparticles' structural, morphological, and optical characteristics are thoroughly described.

2. Experimental part

A collection of fundamental ingredients is needed for the spray and hydrothermal techniques of producing iron oxide, and these elements are essential to the process. First, aluminium chloride (Al_2O_3) and iron chloride hexahydrate ($FeCl_36H_2O$, 99%) are analytical grade and utilised straight away without further purification. After being ultrasonically cleaned in acetone and deionised water, glass substrates are allowed to air dry at room temperature. In order to make the Fe_2O_3 nanoparticle using the hydrothermal technique, 50 mL of deionised water was mixed with 5 mM, 3% Al at 5 mM, 3% Al at 10 mM, and 3% Al at 15 mM of $FeCl_36H_2O$. These processes are consecutive and interrelated. The yellow translucent solution, which served as the precursor solution for Fe_2O_3 nanoparticles, was produced after vigorous stirring at 25 °C for 15 minutes. The precursor solution was put into a stainless-steel autoclave lined with Teflon. The Teflon liner's inner wall was angled against a piece of cleaned glass substrate that had its surface facing down. The stainless-steel autoclave was then annealed for eight hours at 150 degrees Celsius in a furnace. The prepared sample was then removed, carefully cleaned with deionised 10 of 12, and allowed to dry at room temperature. Fe_2O_3 nanoparticles were produced after two hours of annealing at 500 C. Regarding the spraying technique a magnetic stirrer was used to dissolve the initial salt in deionised water at a concentration of 10 mM iron chloride (FeCl3·6H2O hexahydrate) for 15 minutes at 25 °C. Glass slides that had been chemically and ultrasonically cleaned were utilised for deposition. The sprayer was 0.001 m in diameter at the exit. Throughout the spraying procedure, the substrate separation nozzle was kept 30 cm away. The carrier gas was air, and the air pressure was kept constant at 0.50. Throughout the deposition process, the spray rate was maintained at 5 mL/min. Iron (II) oxide doped with Al (Al:Fe_2O_3) was deposited at 350 °C for 60 minutes. For two hours, the nanostructured Al:Fe_2O_3 was heated to 450 °C.

3. Results and discussion

3.1. Structural characterization

The structural study of the created Al-doped Fe_2O_3 thin films was examined using X-Ray diffraction, which was powered by a Cu Kα radiation source (λ = 0.154187 nm) and generated 40 keV and 30 mA at ambient temperature for 2θ values between 25° and 45°. XRD analysis was performed to examine the Al-doped Fe_2O_3 in order to verify the crystallinity of the nanoparticle made using the spraying technique. Two distinct diffraction peaks can be seen at 31.7488º (008), and 33.3324º (107), as shown in Figure 1. These peaks are consistent with the standard XRD data for the Al-doped Fe_2O_3 crystal of ICSD data (01-076-1821). The high crystalline nature of the Al-doped Fe_2O_3 products is shown by the narrow, sharp peaks, suggesting that this is how the high purity of the synthesised Al-doped Fe_2O_3 particles is achieved. The standard diffraction peaks of Al-doped Fe_2O_3 (01-076-1821, ICSD) and the ~~X-ray diffraction (~~XRD~~)~~ patterns of the diffraction peaks of Al doped Fe_2O_3 at various

concentrations generated by hydrothermal technique are shown in Figure.2. At concentrations of 5 mM, 10 mM, and 15 m, respectively, the existence of the peak in the 33.5937º (107), 33.5634º (107), and 33.4295º (107) directions confirms the presence of the other orientation corresponding to the (114) plane, but with modest relative intensities in comparison to the (107) plane. An amorphous sample is identified by its X-ray diffraction pattern at 5mMFe_2O_3:Al. But when concentration rises, the X-ray diffraction peaks are sharper, suggesting that the material's crystallinity has improved. Particle size and distribution alter as concentration rises, potentially producing distinctive structural characteristics like enhanced crystallinity or particle agglomeration. The diameters of the crystallites linked to the XRD data varied from 23.14927 to 23.754 nm. Thus, it is found that the intensity of the (107 diffraction peak) steadily reduces as the precursor concentration ($FeCl_3$ $6H_2O$) grows, and that its half-height breadth lowers as well, leading to an increase in particle size [10]. By examining the captured FE-SEM pictures, the size and shape of the nanoparticles are ascertained.

Since internal stresses and crystallite size have an impact on the line broadening of diffraction peaks, Scherer's equation [11] is used to estimate the approximate crystallite size "D."

$$D = \frac{K\lambda}{\beta ccos\theta} \quad (1)$$

where β is the full width at half maximum (FWHM), λ is the wavelength (0.15418 nm, CuKa), θ is the diffraction angle, and k is the so-called form factor (0.9). The crystallite size was determined using the (107), plane. The (008) plane was selected for the Al-doped Fe_2O_3 sample made by the spray technique, while the (008) plane was used for the Al-doped Fe_2O_3 created by the hydrothermal method.

The Fe_2O_3:Al parameters are: The following relations were used to calculate the dislocation density (δ) and strain (ε) of Al thin films [12].

$$\delta = \frac{1}{D^2} \quad (2)$$

$$\varepsilon = \frac{\beta cos\theta}{4} \quad (3)$$

The findings of the various samples are reported in the table. 1 made it abundantly evident that the values of δ and ε drop as the concentrations of the precursor solution rise. Due to the increase in crystallite size, this is assigned the lower defect level [13].

Table.1. The size of the particles in various synthetic samples.

Samples	β(rad)	D (nm)	δ (cm^{-1})	ε
Synthesized by the spraying **Al: 10mM Fe_2O_3**	0.2362	36.507	0.00 7503	0.20764
Synthesized by the Hydrothermal				
Pure Fe_2O_3	0.3739	23.1492	0.001836	0.309666
Al:5 mM Fe_2O_3	-	-	-	-
Al:10 mM Fe_2O_3	1.0564	8.197687	0.01488	0.879469
Al:15 mM Fe_2O_3	0.3647	23.754	00.001772	0.302335

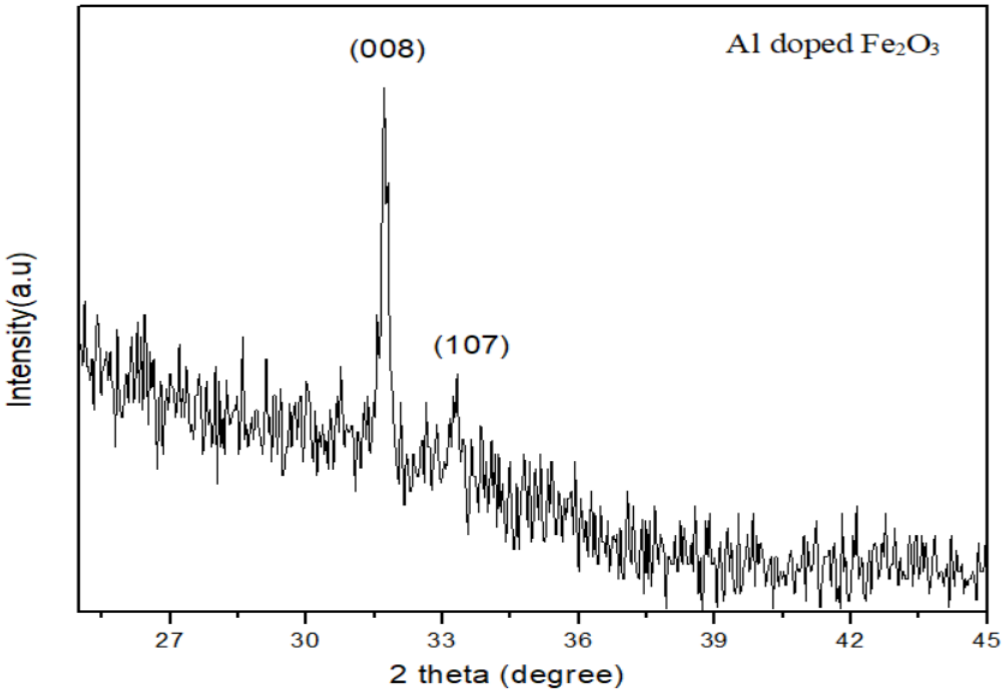

Fig.1. XRD spectra of Fe_2O_3 thin films doped with Al and made using the spraying technique.

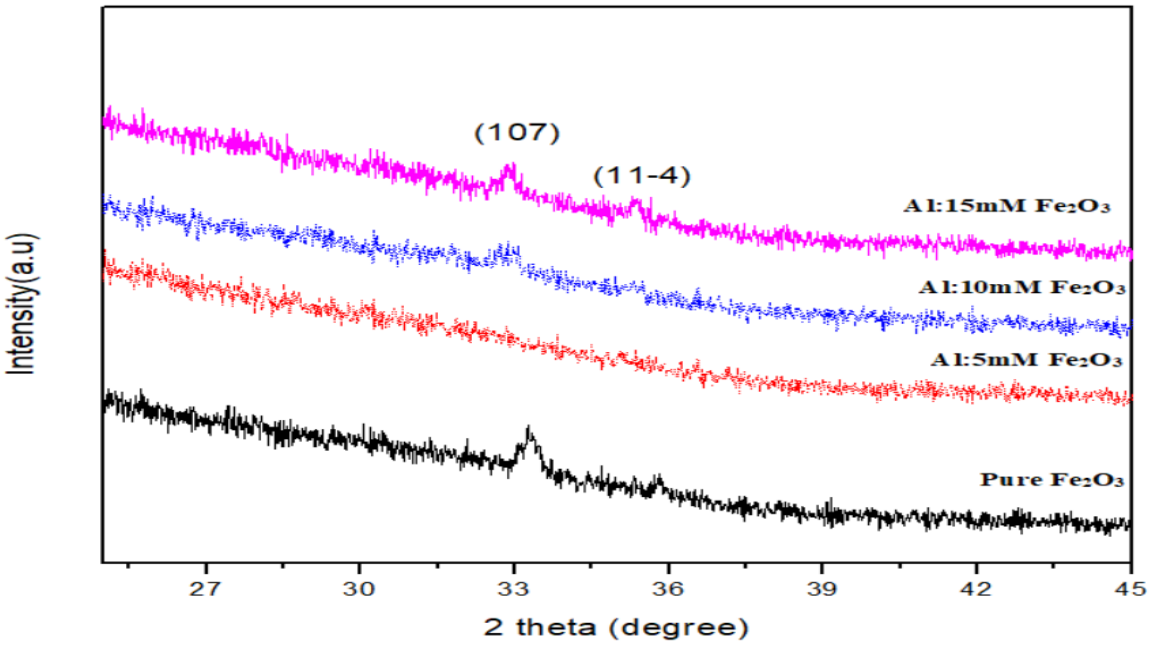

Fig.2. XRD spectra of Fe_2O_3 thin films doped with Al at varying concentrations made using the Hydrothermal process.

3.2. FE-SEM analysis

The FE-SEM pictures of Fe_2O_3 nanoparticles produced with varying hydrothermal concentrations are shown in Figure 3. The spherical Fe_2O_3 nanoparticles exhibited a limited size range of around 42–63 nm and a very homogeneous particle size. Al:15 mM Fe_2O_3 nanoparticles had a tendency to split when the pH was raised. The Al:15 mM Fe_2O_3 nanoparticles' shape did alter; the surface displayed structural characteristics resembling branching, tree-like development in tiny nodules with a variety of nano diameters ranging from 31 to 41 nm. This result is consistent with the XRD findings, indicating that the hydrothermal concentration had an impact on the nanomaterials' size and shape [14].

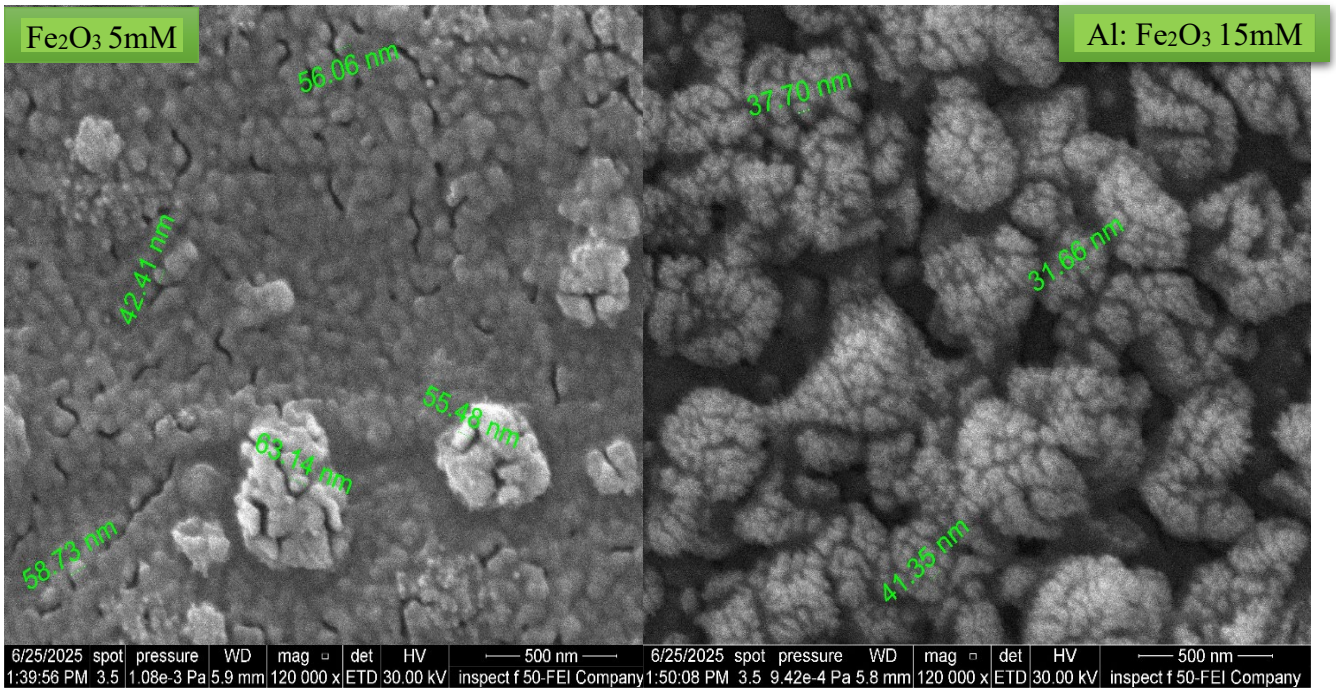

Fig3. FE-SEM pictures of Fe_2O_3 (5 mM) and Al: Hydrothermally produced 15 Mm Fe_2O_3.

3.3 EDS analysis

Chemical analysis using the ~~energy dispersive spectroscopy~~ (EDS~~)~~ approach was used to validate the Fe_2O_3 results. The compositional study of the EDS spectrum of Fe_2O_3 and Al: 15 mM Fe_2O_3 formed by the hydrothermal technique, as shown in Fig. 4, shows that films containing all of the elements Al, Fe, and O as well as other elements like silicon, sodium, calcium, etc., that make up the glass substrate peaks [15].

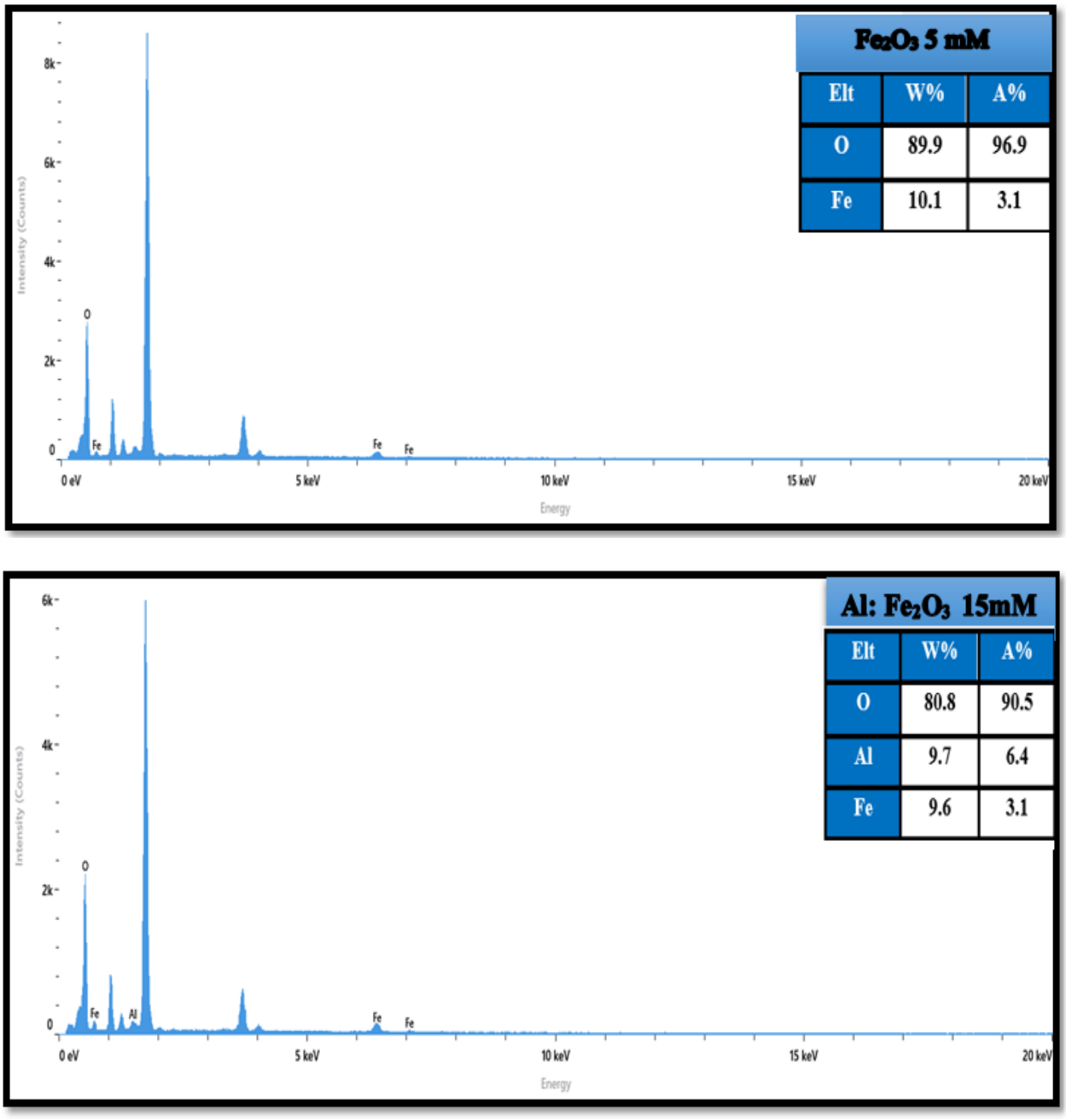

Fig.4. EDX spectra of Fe_2O_3 and Al: Hydrothermally produced 15Mm Fe_2O_3.

3.4. Optical Properties

UV-Visible spectroscopy is employed to analyze thin films by measuring their absorption of ultraviolet and visible light. This technique provides valuable insights into the optical properties of the films, such as light absorption and transmittance, aiding in the understanding of their interaction with light and the evaluation of their optical behavior. All of the absorption curves for Al:Fe_2O_3 synthesized with varying precursor concentrations show a strong absorption in the 340–900 nm wavelength range, according to the absorption spectra in the UV-Vis range in (Fig.5) . A distinctive absorption peak at around 350–600 nm was seen in the films made using the sputtering technique in (Fig.7). The films with Al:5 mM Fe_2O_3 concentration had high transmittance > 60% in the UV-Vis areas, according to the transmittance spectra shown in (Fig. 6) and (Fig.8). In contrast, films with varied concentrations have low transmittance ~40% in the UV region but rose to > 60% in the Vis region. Here, it is evident that transmittance drops as concentration rises. This outcome is in line with findings from other research [16–17].

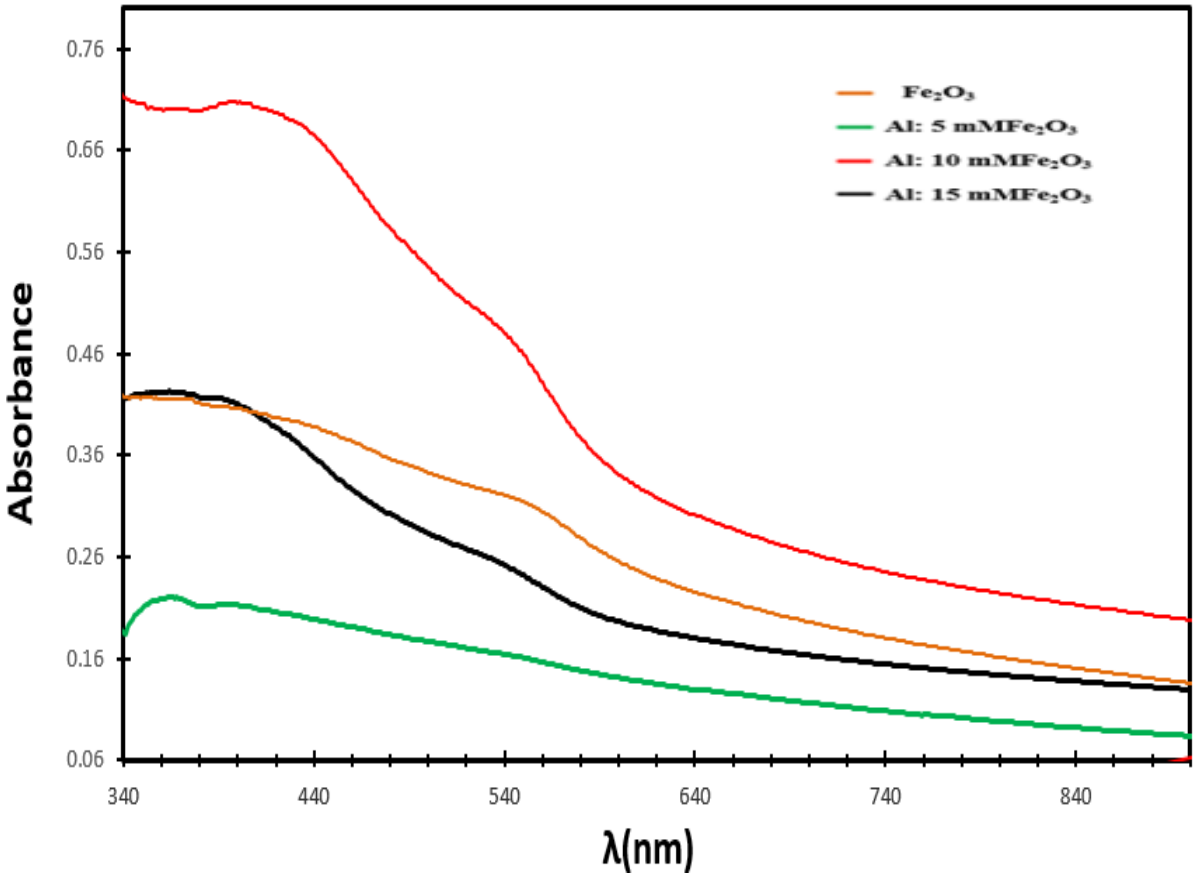

Fig.5. Absorption spectra of Al doped Fe_2O_3 at varying concentrations acquired by the Hydrothermal technique.

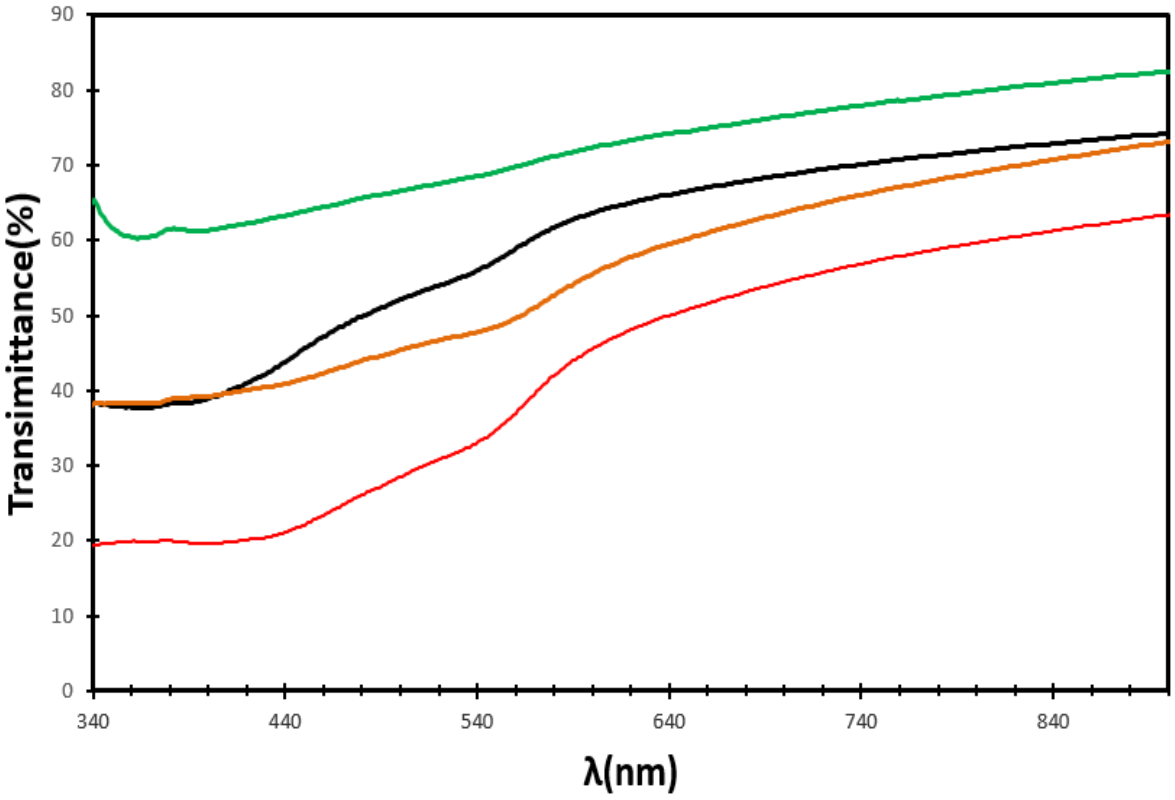

Fig.6. Transmittance spectra of Al-doped Fe_2O_3 at varying concentrations acquired using the Hydrothermal technique.

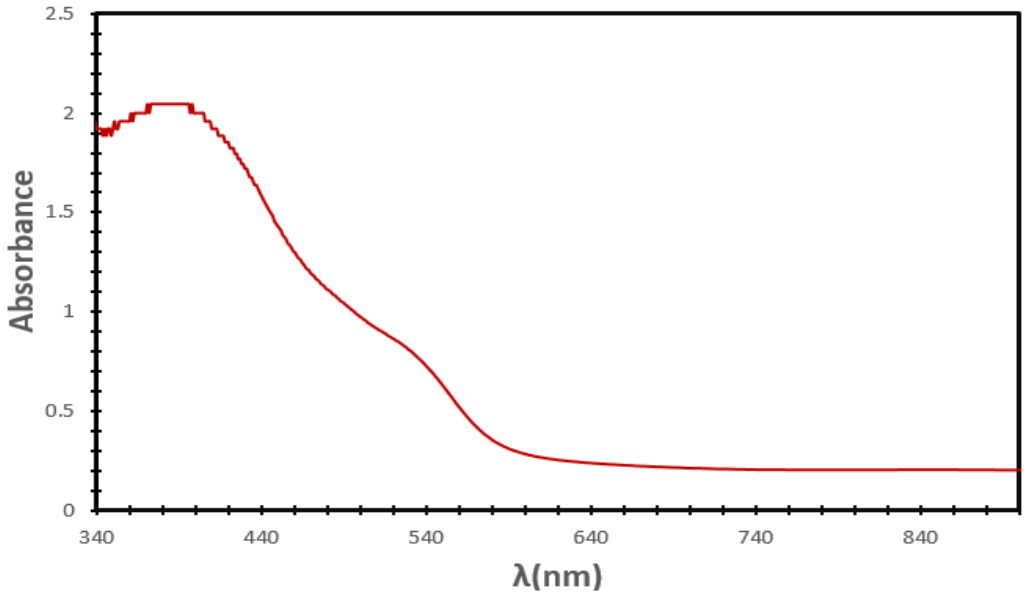

Fig.7. Absorption Spectra of Al-doped Fe_2O_3 obtained through the spraying method.

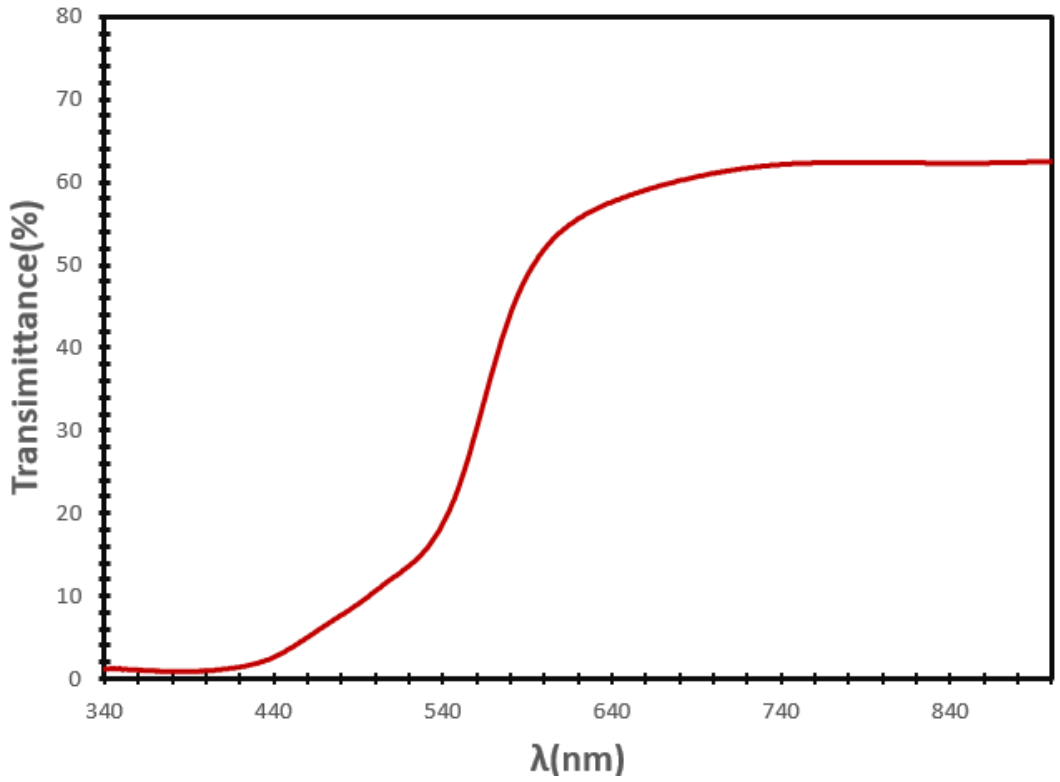

Fig.8. Transmittance Spectra of Al-doped Fe_2O_3 obtained through the spraying method.

The absorption edge, which is provided by the following equation, may be extrapolated to estimate the optical band gap (**E_g**) for Al:Fe_2O_3 nanoparticles. The formula[18].

$$\alpha h\nu = A(h\nu - E_g)^n \quad (4)$$

where, depending on the kind of electron transfer, **n** is a constant, **hυ** is the energy of light, **A** is a constant, and **α** is the absorption coefficient. The bandgap of Fe_2O_3:Al is straight (n=2). The plot of **$(\alpha h\upsilon)^2$** against **hυ** is shown in (Fig. 9). The linear absorption edge part's intercept with the energy axis may be used to determine the energy gap. The photon energy is **E_g** when **$(\alpha h\upsilon)^2$** is zero. The optical bandgap of (1.9–2.3) eV is increased by the reduction in particle size of Fe_2O_3:Al synthesized with varying concentrations of precursor, where they have an inverse connection. Moreover, the results indicate that the optical band gap of Fe_2O_3 nanoparticles is 1.95 eV, which is lower than the recorded band gap of pure Fe_2O_3 nanoparticles, estimated at 2.2 eV, as reported in references [19–20]. This reduction serves as additional evidence for the presence of intrinsic oxygen vacancies in the nanoparticles synthesized via the hydrothermal method. The graph of the direct transitions of the films made using the spraying approach is shown in Fig. 10. 2.19 eV is the straight band gap energy value. This is comparable to what has been shown in other research [21].

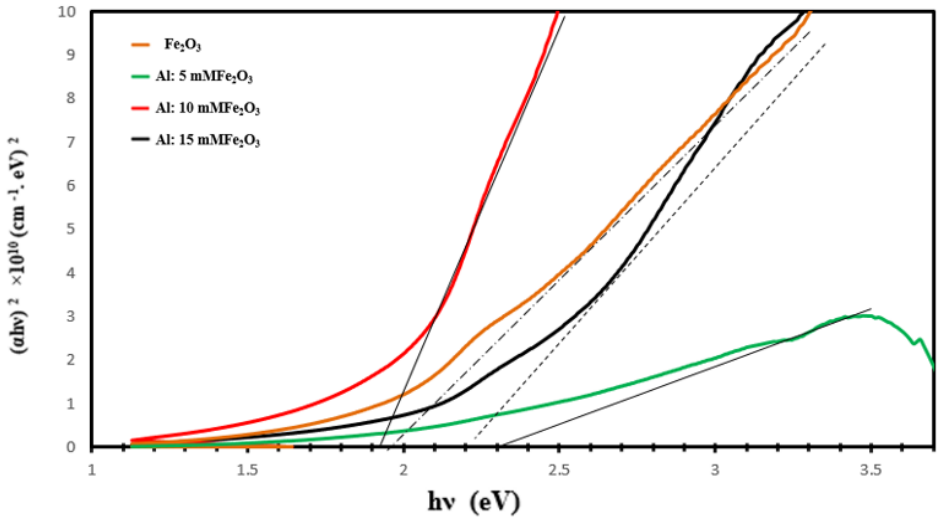

Fig.9. The Hydrothermal process employing varying concentrations produced a tauc plot with the UV-Vis DRS spectra of Al-doped Fe_2O_3.

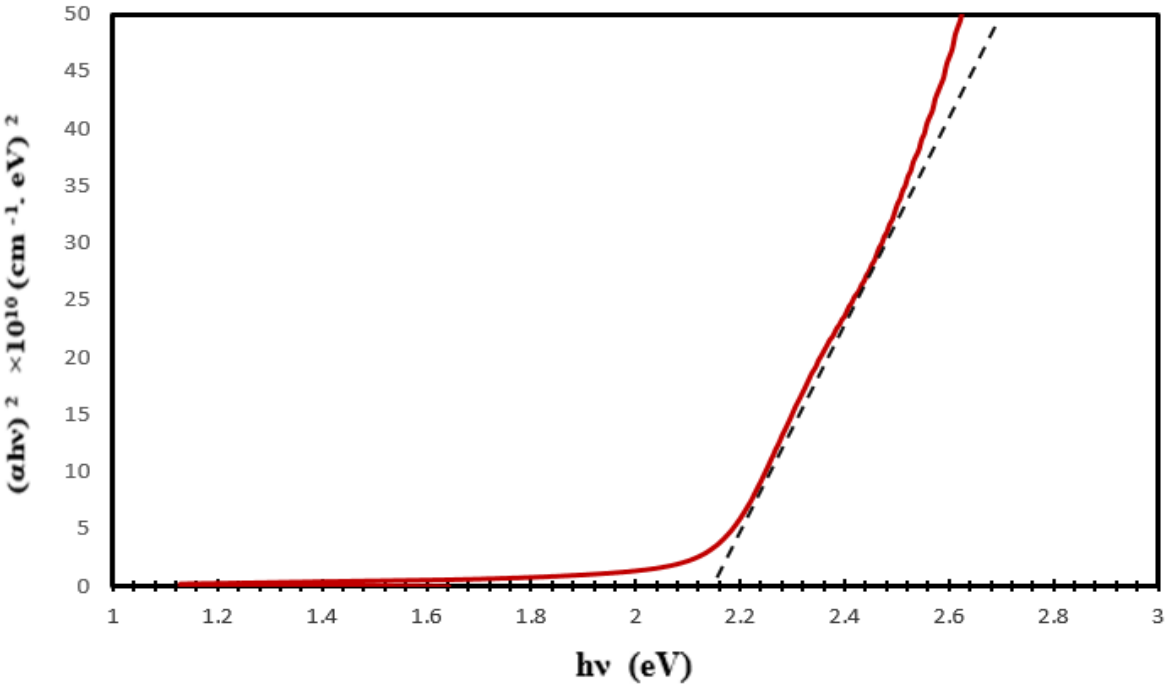

Fig.10. The UV-Vis DRS spectra of Al-doped Fe_2O_3 produced by the spraying approach are shown in the tauc plot.

4. Conclusion

The existence of aluminum with Fe_2O_3 was verified by the XRD, FE-SEM, and EDS analyses. UV-Vis spectroscopy made it abundantly evident that a change in concentration had a substantial impact on the broader energy band of Fe_2O_3. For pure Fe_2O_3 produced by the hydrothermal technique, the direct band gap energy was 1.95 eV. For 5, 10, and 15 mM Al: Fe_2O_3, this demonstrated changes of 2.3, 1.92, and 2.2 eV. The spraying approach has been successfully used to create iron oxide of Al-doped Fe_2O_3. The sample's band gap was determined to be 2.19 eV. In conclusion, the two primary techniques for preparing different materials spraying and hydrothermal produce goods with unique qualities and are used in a variety of cutting-edge industrial applications. These techniques all provide exact control over preparation factors, which affect crop yields both chemically and physically. The spraying technique is crucial for creating vast amounts of nanomaterials since it can accurately alter their structure and composition, opening up a wide range of applications in industries like electronics, where it is used to make sensors and solar panels. On the other hand, the hydrothermal approach improves surface reaction and chemistry processes by creating the perfect conditions for the formation of nanomaterials via high pressure and high temperatures.

References

[1] O. Milošević, L. Mančić, M. E. Rabanal, S. Ohara, (2013). In EUROMAT 2013: European Congress and Exhibition on Advanced Materials and Processes, Sevilla 8-13, October, 2013: CD Book of Abstracts. FEMS.
[2] M. M. Kareem, Z. T. Khodair, F. Y. Mohammed. Journal of Ovonic Research. **16**(1), 53–61 (2020). https://doi.org/10.15251/JOR.2020.161.53
[3] Y. Al-Douri, N. Amrane, M. R. Johan. Journal of Materials Research and Technology. **8**(2), 2164–2169 (2019). https://doi.org/10.1016/j.jmrt.2019.02.004
[4] A. Manikandan, A. Saravanan, S. A. Antony, M. Bououdina. Journal of Nanoscience and Nanotechnology. **15**(6), 4358–4366 (2015). https://doi.org/10.1166/jnn.2015.9804
[5] C. Xia, Y. Jia, M. Tao, Q. Zhang. Physics Letters A. **377**(31–33), 1943–1947 (2013). https://doi.org/10.1016/j.physleta.2013.05.026
[6] W. H. Eisa, N. Okasha. Journal of Scientific Research in Science, 37(1), 73–91. (2020). https://doi.org/10.3390/cryst13111601
[7] A. B. Taha, M. S. Essa, B. T. Chiad. Journal of Metastable and Nanocrystalline Materials. 35, 1–10 (2023). https://doi.org/10.3390/nano14151263
[8] N. Zhao, C. He, J. Liu, H. Gong, T. An, H. Xu, F. Zhao, R. Hu, H. Ma, J. Zhang. Journal of SolidState Chemistry, **219**, 67–73 (2014). https://doi.org/10.1016/j.jssc.2014.06.039
[9] Z. Wang, T. F. Zhang, Z. Ge, Y. J. Luo. Chinese Chemical Letters. **26**(12), 1535–1537 (2015). https://doi.org/10.1016/j.cclet.2015.07.017
[10] A. Lassoued, B. Dkhil, A. Gadri, S. Ammar. Results in Physics, **7**, 3007–3015 (2017). https://doi.org/10.1016/j.rinp.2017.07.066
[11] F. Y. Mohammed, C. H. Kareem, F. G. Hammoodi, M. H. Al-Timimi. Digest Journal of Nanomaterials and Biostructures. **20**(3), 965–973(2025). https://doi.org/10.15251/DJNB.2025.203.965
[12] F. G. Hammoodi, A. A. Shuihab, S. A. Ebrahiem. AIP Conference Proceedings. **2394**(1). 23-24 (2022). https://doi.org/10.1063/5.0122507
[13] P. D. More, P. R. Jadhav, A. A. Ghanwat, I. A. Dhole, Y. H. Navale, V. B. Patil. Journal of Materials Science: Materials in Electronics. **28**(23), 17839–17848 (2017). https://doi.org/10.1007/s10854-017-7725-5
[14] F. Afshari, E. Mandev, S. Rahimpour, B. Muratçobanoğlu, B. Şahin, E. Manay, R. Teimuri-Mofrad. Microfluidics and Nanofluidics. **27**(4), 26 (2023). https://doi.org/10.1007/s10404-023-02637-4
[15] M. Sharmin, J. Podder. Semiconductor Science and Technology. **34**(7), 075033 (2019). DOI: 10.1088/1361-6641/ab2790
[16] A. B. C. Ekwealor, F. I. Ezema. Journal of Ovonic Research. 9, 35–43 (2013).

[17] S. Sivakumar, D. Anusuya, C. P. Khatiwada, J. Sivasubramanian, A. Venkatesan, P. Soundhirarajan. Spectrochimica Acta Part A: Molecular and Biomolecular Spectroscopy. **128**(15), 69–75 (2014). https://doi.org/10.1016/j.saa.2014.02.136
[18] A. Y. Ibrahim, F. G. Hammoodi. Journal of Nanostructures. **15**(1), 229–238 (2025). https://doi.org/10.22052/JNS.2025.01.022
[19] M. A. Mohamed, N. A. Rahman, M. F. M. Zain, L. J. Minggu, M. B. Kassim, J. Jaafar, S. Samad, M.S.Mastuli, R. J. Wong. Journal of Alloys and Compounds. **820**(15), 153143 (2020). https://doi.org/10.1016/j.jallcom.2019.153143
[20] J. Liu, Y. Y. Cai, Z. F. Tian, G. S. Ruan, Y. X. Ye, C. H. Liang, G. S. Shao. Nano Energy. **9**, 282-290 (2014). https://doi.org/10.1016/j.nanoen.2014.08.005
[21] B. Samira, K. G. Chandrappa, B. A. H. Sharifah. Research Journal of Chemical Sciences. **3**(7), 62–68 (2013).